Supplementary material to:

Seasonal climate signals preserved in biochemical varves: insights from novel high-resolution sediment scanning techniques

Paul D. Zander[1*], Maurycy Żarczyński[2], Wojciech Tylmann[2], Shauna-kay Rainford[3], Martin Grosjean[1]

[1] *Institute of Geography & Oeschger Centre for Climate Change Research, University of Bern, Bern, Switzerland*

[2] *Faculty of Oceanography and Geography, University of Gdansk, Poland*

[3] *Institute of Plant Sciences & Oeschger Centre for Climate Change Research, University of Bern, Bern, Switzerland*

[*] Correspondence: E-mail address: paul.zander@giub.unibe.ch

Table S1. Summary of split-period validation statistics. RE = reduction of error, CE = coefficient of efficiency, RMSE = root mean square error of prediction. RE and CE were calculated according to Cook et al. (1994).

Target variable	Calibration period	Verification period	R^2_{adj}	RE	CE	RMSE
MAMJJA temperature	1966-1992	1993-2019	0.39	0.75	0.30	0.68 ° C (14.1%)
MAMJJA temperature	1993-2019	1966-1992	0.35	0.67	0.15	0.80 ° C (16.7%)
Mar-Dec wind days	1966-1991	1992, 1995-2019	0.30	0.61	-3.94	7.34 days (22.9%)
Mar-Dec wind days	1992, 1995-2019	1966-1991	0.15	-0.28	-3.22	15.35 days (48.0%)

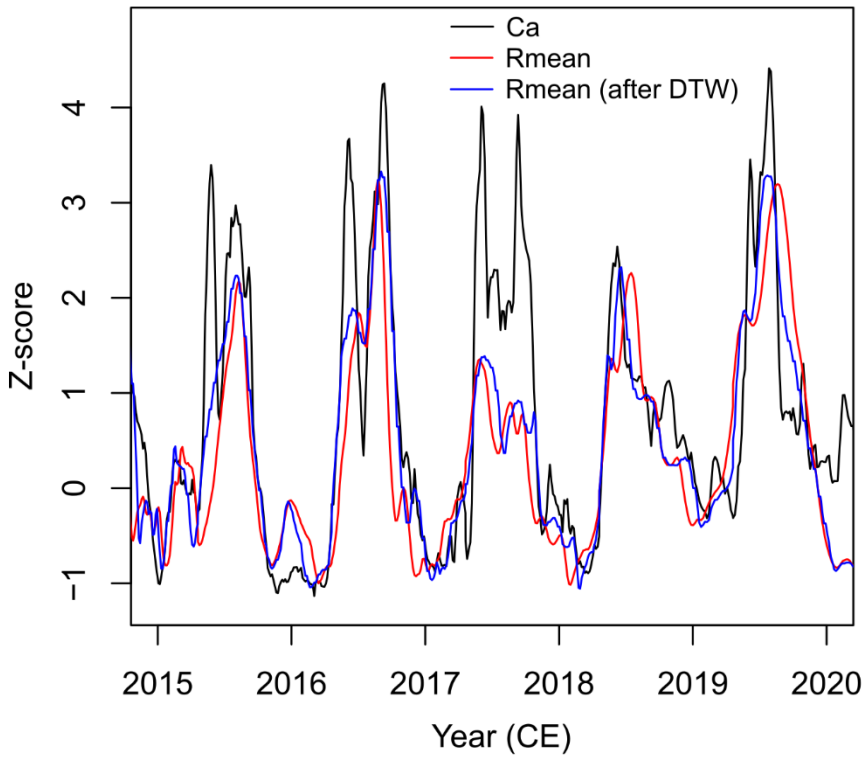

Figure S1. Example of the effect of dynamic time warping alignment used to align HSI and μXRF data at the sub-varve scale. Red line shows Rmean plotted on varve age scale from varve counting on HSI image. Blue line shows the same data after alignment to the Ca μXRF data. This new alignment was then applied to Bphe and TChl data from HSI before any other analyses.

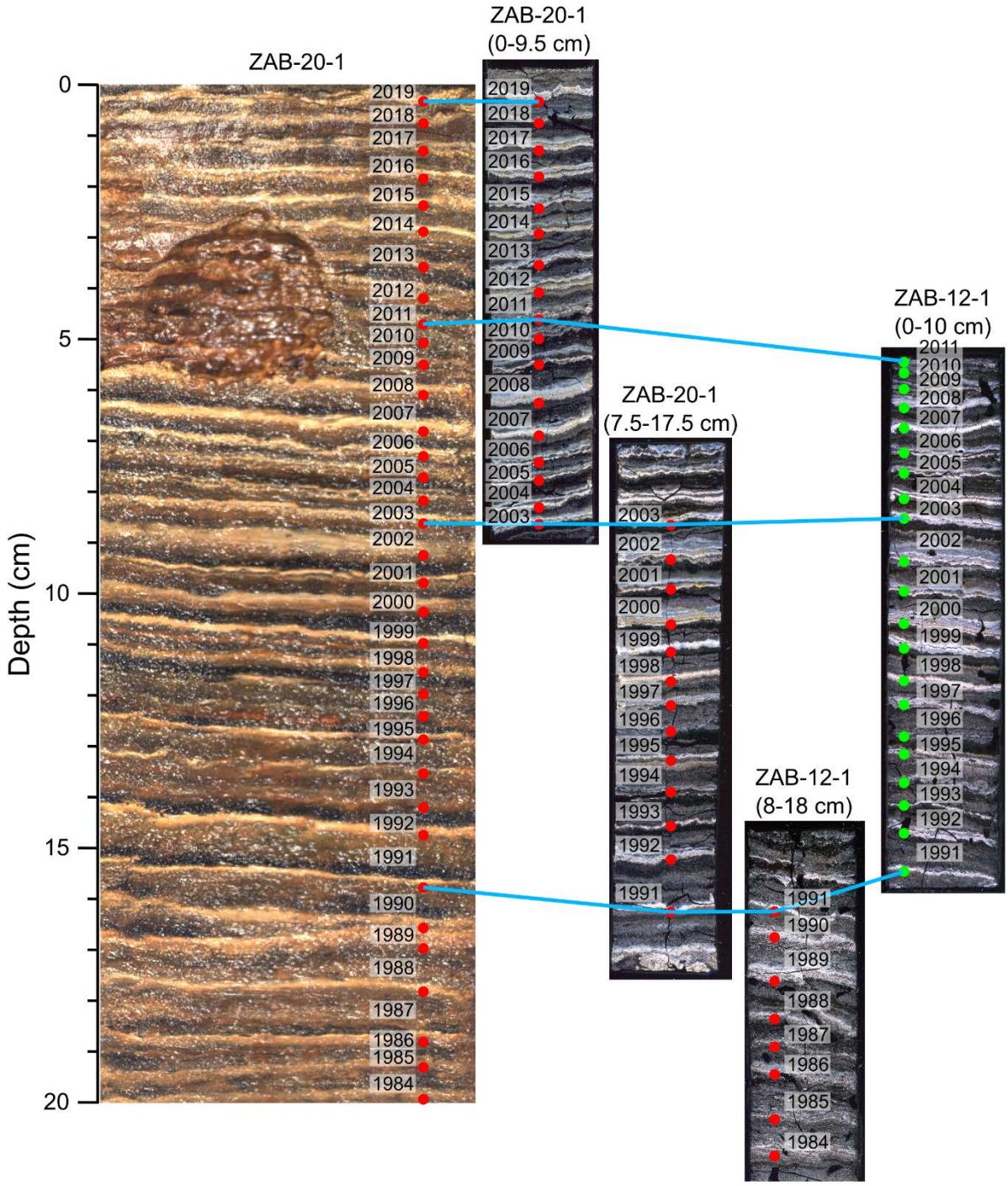

Figure S2. Varve count results shown on core images (ZAB-20-1) and resin-embedded slabs (ZAB-12-1 and ZAB-20-1). Green dots indicate varve counts done on resin-blocks that were not used for analyses in this study, but were used to confirm the varve count.

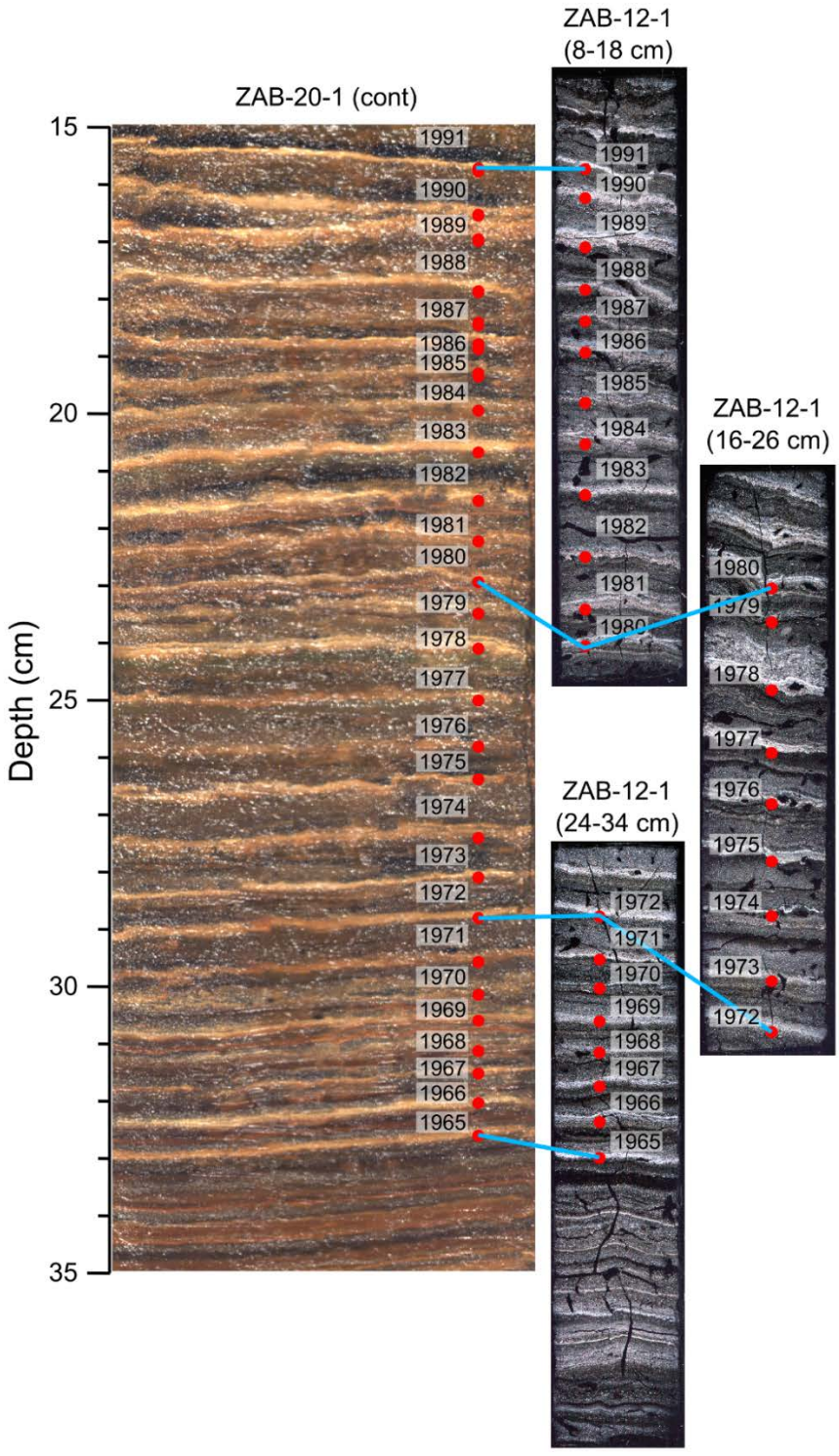

Figure S2 (cont). Varve count results shown on core images (ZAB-20-1) and resin-embedded slabs (ZAB-12-1 and ZAB-20-1).

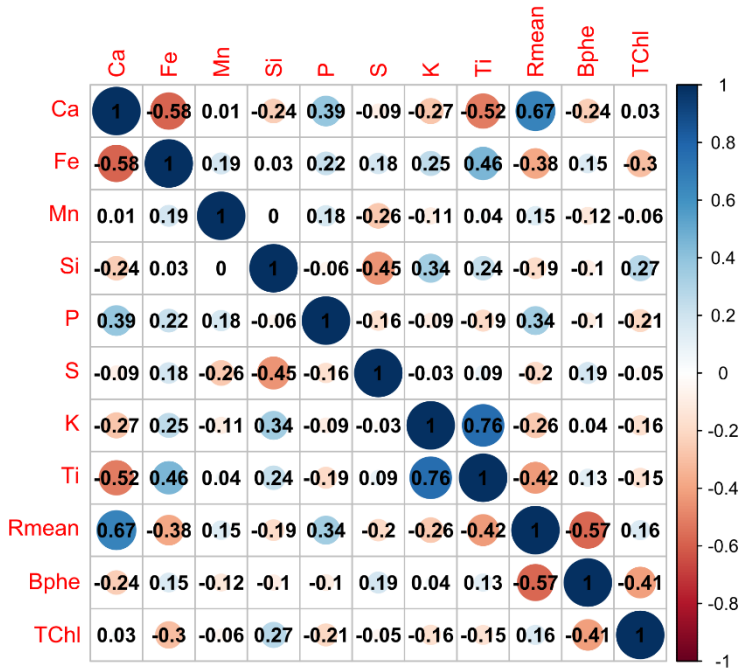

Figure S3. Correlation plot of high-resolution spectroscopy imaging data at original resolution (60 µm, n = 5631).

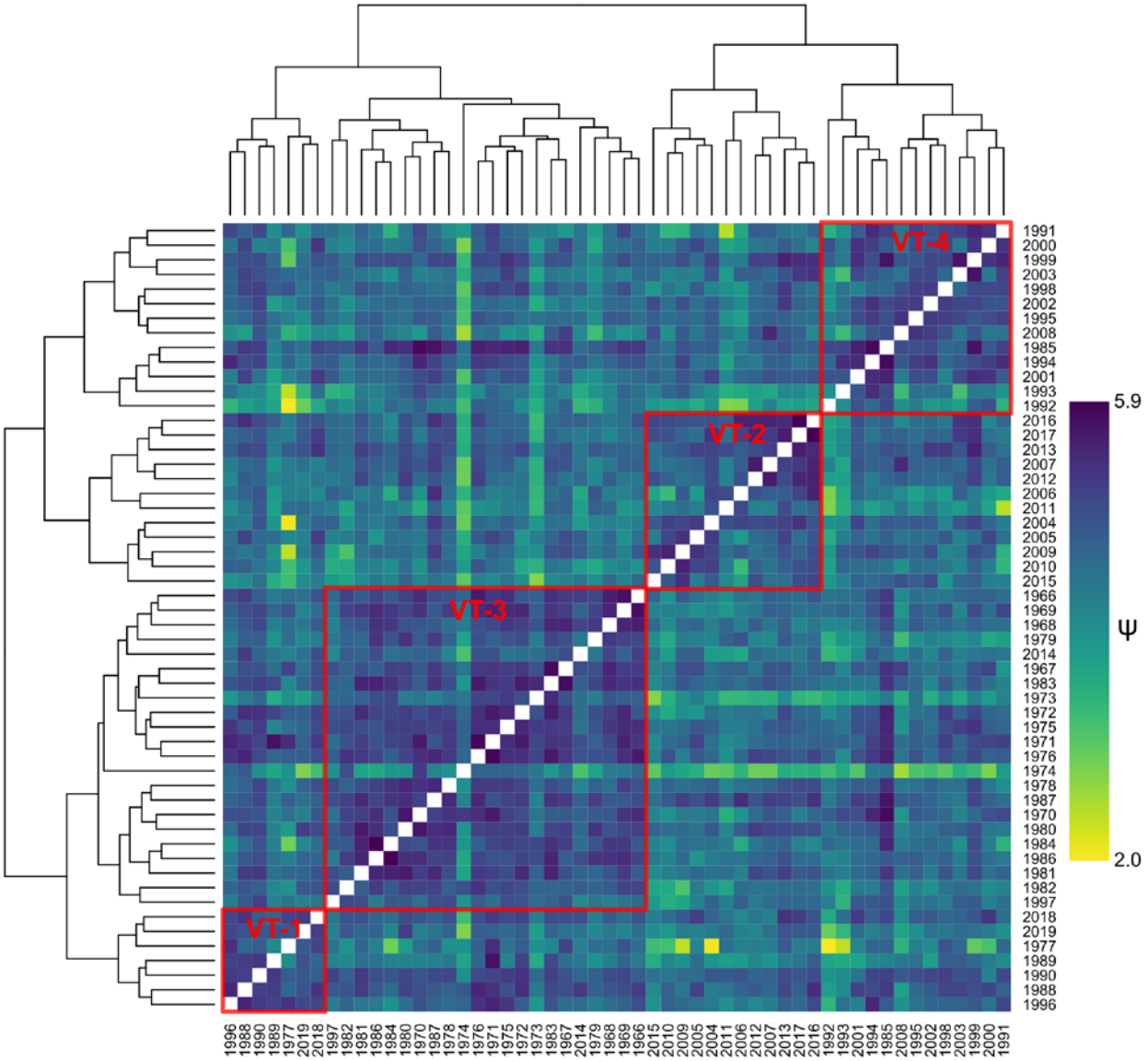

Figure S4. Matrix of dissimilarity values psi (ψ) and dendrogram resulting from hierarchical clustering. Red boxes identify varve type (VT) clusters.

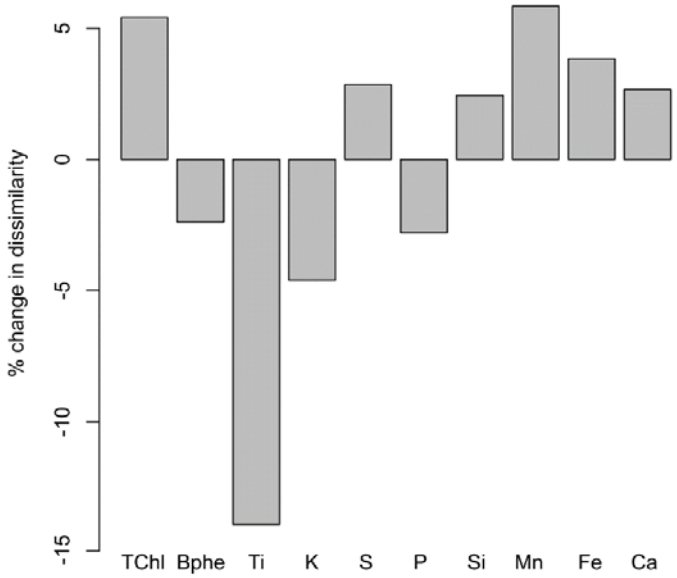

Figure S5. Percent change in dissimilarity (ψ) attributed to each variable. Positive values indicate the variable contributes to year-to-year dissimilarity in annual time series. Negative values indicate that the variable contributes to year-to-year similarity in annual time series.

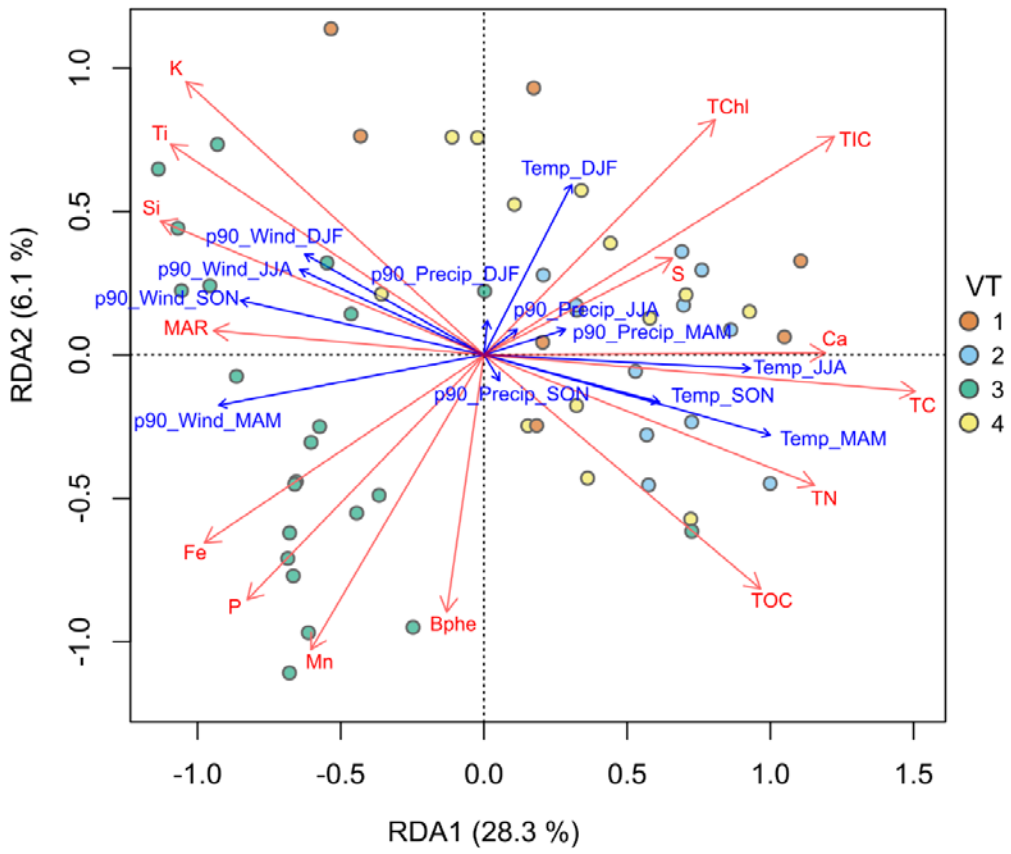

Figure S6. Results of a Redundancy Analysis (RDA) with mean annual proxy data as response variables and seasonal meteorological data as explanatory variables.

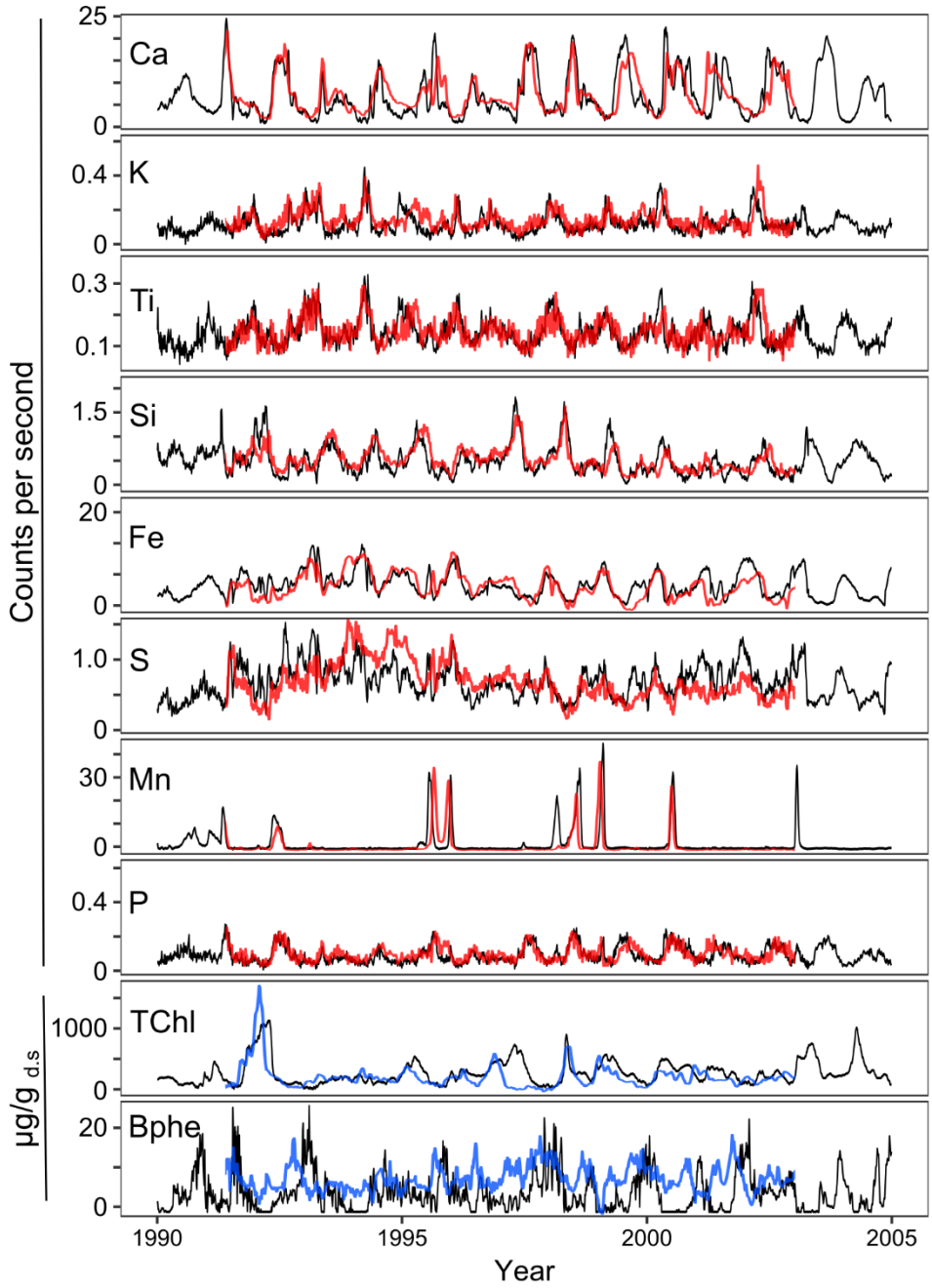

Figure S7. Plot demonstrating reproducibility of high-resolution scanning data by measurement of overlapping sections from different cores. Black lines represent data used in this study. Red lines represent an overlapping segment of the ZAB-12-1 core that was not used in the composite data for this study. Blue lines represent HSI data from an additional core (ZAB-19-1) not used for other analyses in this study.

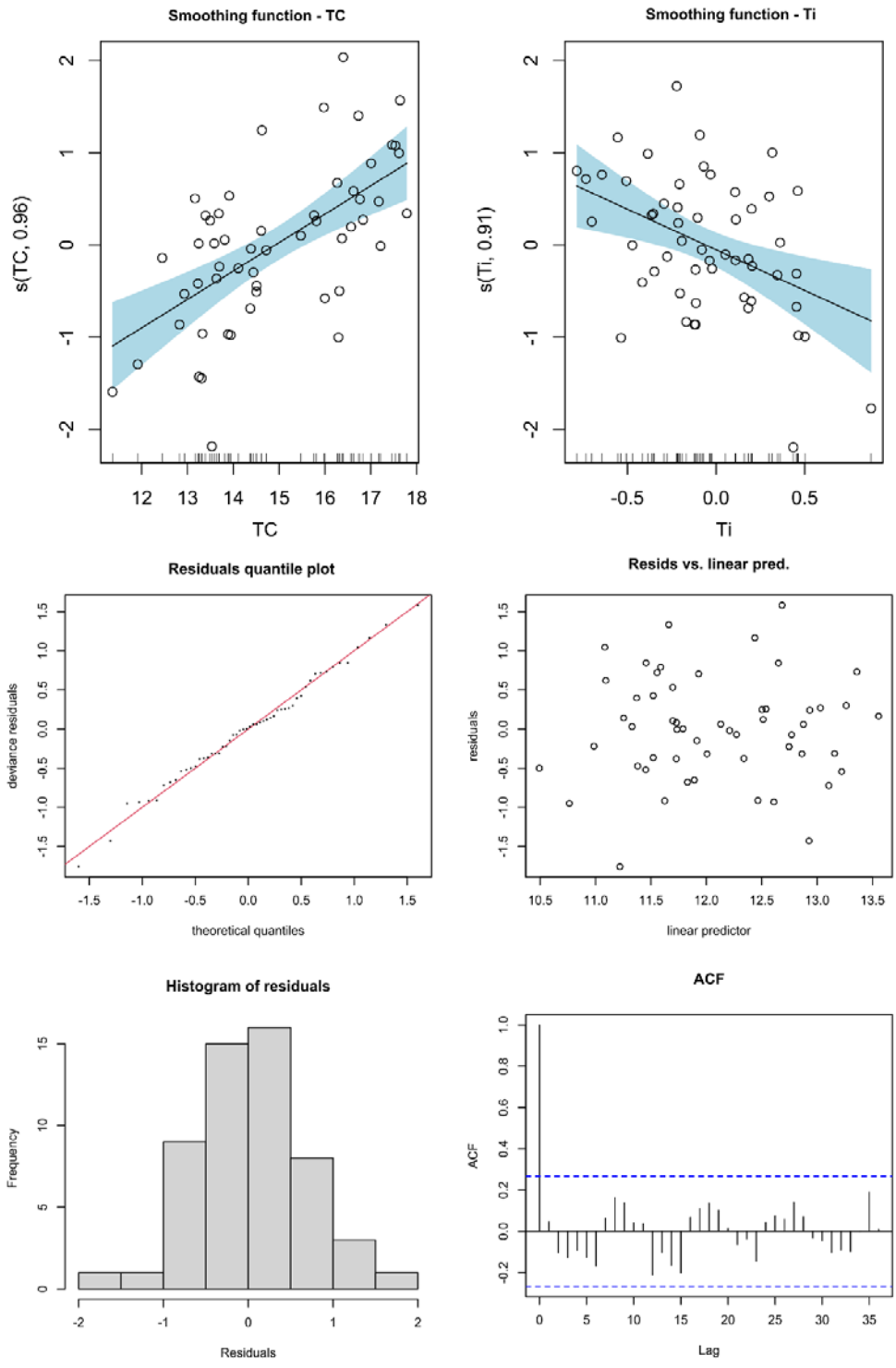

Figure S8. Partial effect plots and diagnostic plots for spring and summer temperature GAM reconstruction fit with TC and Ti.

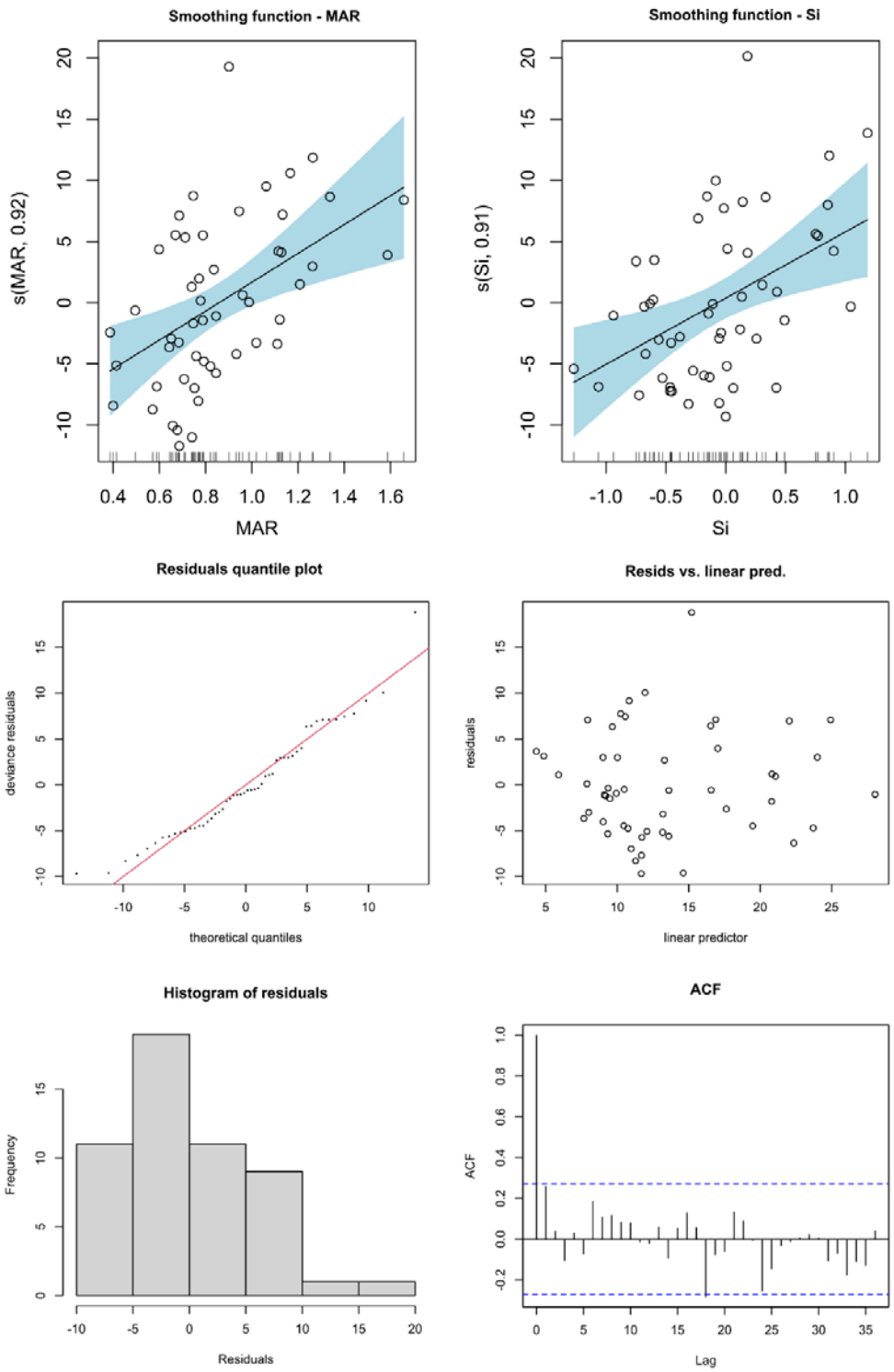

Figure S9. Partial effect plots and diagnostic plots of Mar-Dec wind days GAM reconstruction fit with MAR and Si.

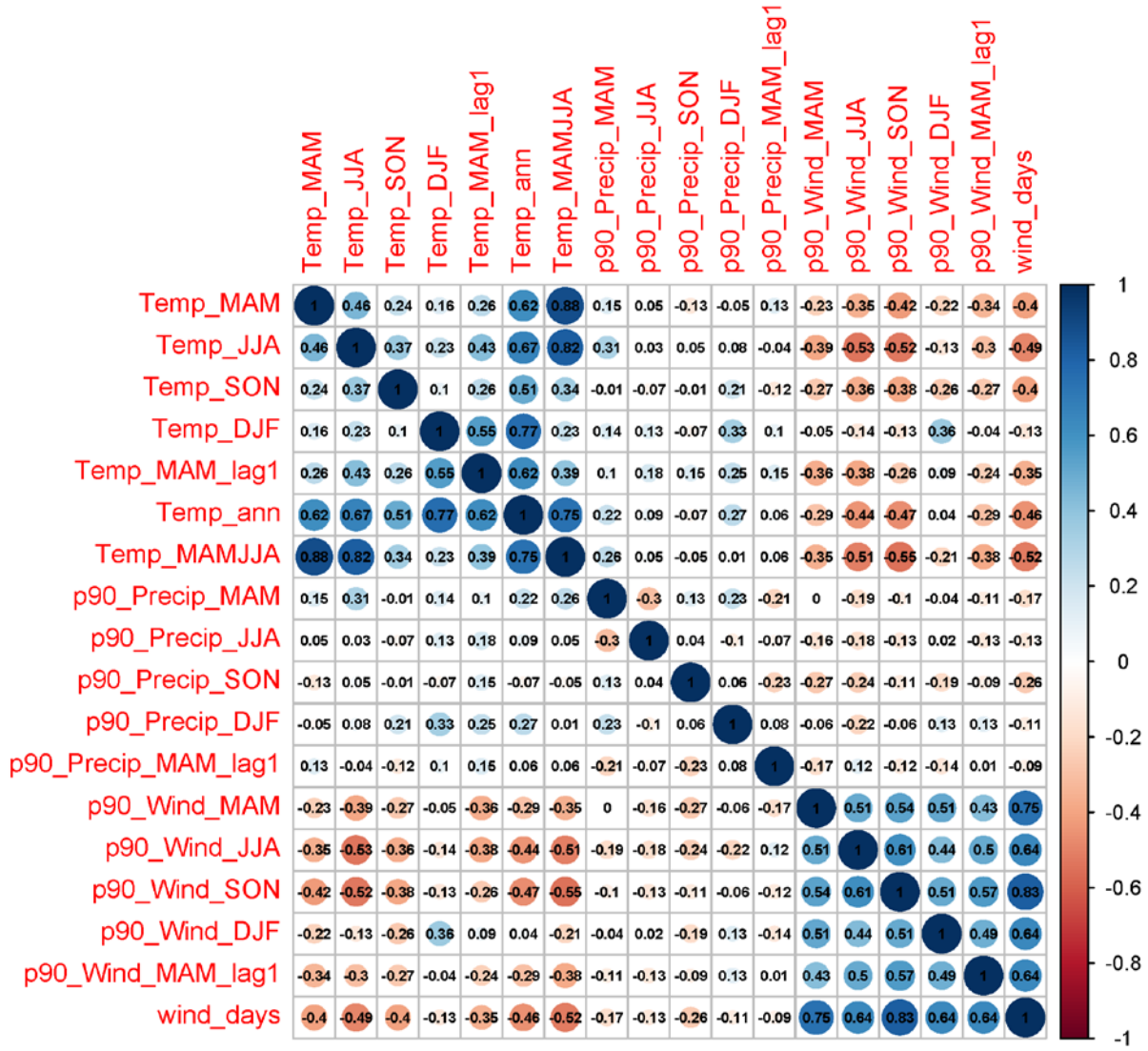

Figure S10. Correlation plot of selected meteorological variables.

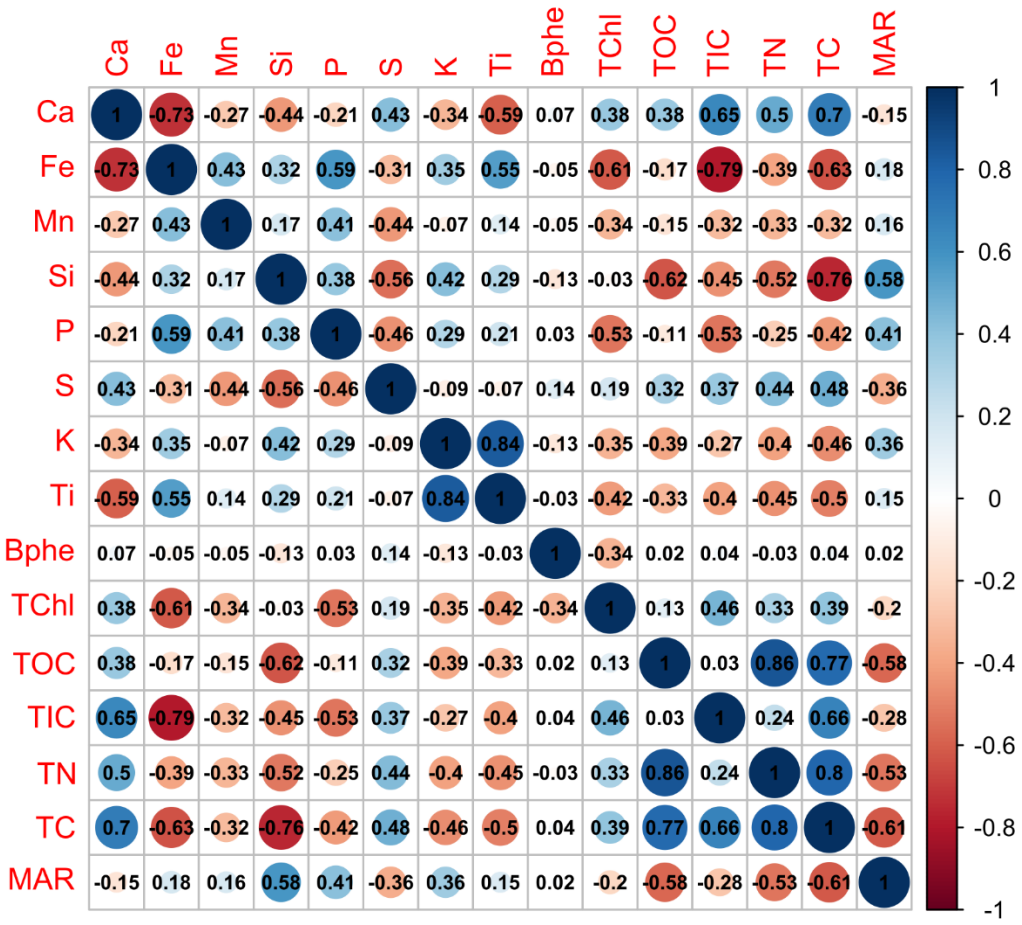

Figure S11. Correlation plot of proxy data at annual resolution (mean annual values, n = 54).